Journal of Rock Mechanics and Geotechnical Engineering 12 (2020) 461–472

Contents lists available at ScienceDirect

Journal of Rock Mechanics and Geotechnical Engineering

journal homepage: www.jrmge.cn

Full Length Article

Controlling effects of differential swelling index on evolution of coal permeability

Chuanzhong Jiang [a,b], Zhenfeng Zhao [c], Xiwei Zhang [a], Jishan Liu [d,*], Derek Elsworth [e], Guanglei Cui [a]

[a] Key Laboratory of Ministry of Education on Safe Mining of Deep Metal Mines, Northeastern University, Shenyang, 110819, China
[b] Beijing Key Laboratory for Precise Mining of Intergrown Energy and Resources, China University of Mining and Technology, Beijing, 100083, China
[c] Oil & Gas Technology Research Institute, Changqing Oilfield Company, Xi'an, 710018, China
[d] Department of Chemical Engineering, School of Engineering, The University of Western Australia, 35 Stirling Highway, Crawley, WA, 6009, Australia
[e] Department of Energy and Mineral Engineering, G3 Centre and Energy Institute, The Pennsylvania State University, University Park, PA16802, USA

ARTICLE INFO

Article history:
Received 23 November 2019
Received in revised form
27 January 2020
Accepted 5 February 2020
Available online 8 April 2020

Keywords:
Coal permeability
Differential swelling behavior
Gas adsorption
Equilibrium pressure

ABSTRACT

Coal permeability measurements are normally conducted under the assumption that gas pressure in the matrix is equalized with that in fracture and that gas sorption-induced swelling/shrinking strain is uniformly distributed within the coal. However, the validity of this assumption has long been questioned and differential strain between the fracture strain and the bulk strain has long been considered as the primary reason for the inconsistency between experimental data and poroelasticity solutions. Although efforts have been made to incorporate the impact into coal permeability models, the fundamental nature of those efforts to split the matrix strain between fracture and coal bulk remains questionable. In this study, a new concept of differential swelling index (DSI) was derived to theoretically define the relation among sorption-induced strains of the coal bulk, fracture, and coal matrix at the equilibrium state. DSI was a function of the equilibrium pressure and its magnitudes were regulated by the Langmuir constants of both the matrix and the coal bulk. Furthermore, a spectrum of DSI-based coal permeability models was developed to explicitly consider the effect of differential strains. These models were verified with the experimental data under the conditions of uniaxial strain, constant confining pressure, and constant effective stress.

1. Introduction

As an "unconventional" gas resource, coalbed methane (CBM) is a natural product of coalification process (Moore, 2012). CBM has long been considered as a source of disasters for underground coal mining, but now is recognized as a valuable energy resource (Flores, 1998). Therefore, reasonable disposal of CBM released from underground coal mining can not only reduce gas explosion hazard but also recover this clean energy. Depending on reservoir conditions, CBM can be extracted using reservoir-pressure depletion method or enhanced CBM (ECBM) recovery methods. For ECBM, nitrogen (N_2) and/or carbon dioxide (CO_2) are injected into coal seam to desorb and displace CBM (Puri and Yee, 1990; Gunter et al., 1997).

One of the key reservoir parameters for CBM production and CO_2 sequestration in coal seams is coal permeability. Gas is mainly stored in a form of adsorption in coal seams, and both CBM recovery and CO_2 injection trigger a series of desorption or adsorption associated processes in the coal seams (Chen et al., 2012; Perera et al., 2013). During CBM production, the fracture pressure drawdown induces gas desorption from the coal matrix, and the desorbed gas flows into the fracture network. During desorption, the coal matrix shrinks. As a direct consequence of this matrix shrinkage, the fractures may dilate, and fracture permeability increases correspondingly (e.g. Harpalani and Schraufnagel, 1990a). Conversely, CO_2 geological sequestration and CO_2-ECBM may reverse these processes.

Significant experimental efforts have been made to investigate the characteristics of coal permeability evolution. Coal permeability experiments can be generally divided into stress-controlled

* Corresponding author.
E-mail address: jishan.liu@uwa.edu.au (J. Liu).
Peer review under responsibility of Institute of Rock and Soil Mechanics, Chinese Academy of Sciences.

https://doi.org/10.1016/j.jrmge.2020.02.001

(constant confining pressure and constant effective stress) and displacement-controlled ones (uniaxial strain condition and constant volume condition) (Shi et al., 2018). Under following four boundary conditions, permeability shows different evolution characteristics:

(1) Laboratory-measured coal permeability in terms of adsorbing gasses such as CH_4 and CO_2 can change from reduction to enhancement instantaneously under constant confining pressure condition (Robertson, 2005; Pini et al., 2009; Siriwardane et al., 2009; Wang et al., 2011, 2019; Vishal et al., 2013).
(2) Most experimental data (Connell et al., 2010a; Lin and Kovscek, 2014; Meng et al., 2015; Chen et al., 2019; Wei et al., 2019a) exhibit significant changes under constant effective stress condition: the permeability declines initially and then remains stable as the gas pressure increases.
(3) An ingenious experimental work was conducted by Mitra et al. (2012). In their experiment, coal sample was held under uniaxial strain condition. The coal sample was taken from San Juan basin. It was not permitted to shrink laterally as a result of gas desorption by adjusting the confining pressure. The results showed that coal permeability increases continuously with decrease in gas pressure. These observations are consistent with the field observations made in different parts of the San Juan basin (Gierhart et al., 2007).
(4) A permeability test for coal was conducted under constant volume condition to investigate the coal–cleat interactions using helium (Wang et al., 2017). The results showed that permeability increases as the pore pressure increases.

Various coal permeability models have been proposed to explain the variability of coal permeability under laboratory or field conditions. Based on applicable boundary conditions, major coal permeability models were classified into two groups (Liu et al., 2011a): permeability models under conditions of uniaxial strain and that under conditions of variable stress. In these models (Gray, 1987; Palmer and Mansoori, 1996; Shi and Durucan, 2003b), coal permeability is defined as a function of the coal bulk strain. It is also assumed that the coal bulk strain caused by gas adsorption is equal to that of the fracture (Cui et al., 2007; Zhang et al., 2008). However, this assumption may not be valid for coal (Zang et al., 2015).

This discrepancy between assumption and reality has long been recognized. In the study (Liu et al., 2010a), the concept of "internal swelling stress" was introduced to account for the impact of matrix swelling/shrinkage on the fracture aperture changes. In this study, the matrix strain was divided into two parts: one for the fracture component and the other for the bulk strain. Based on this concept, permeability models under conditions of uniaxial strain and constant external stress were developed.

In other studies (e.g. Connell et al., 2010a; Lu and Connell, 2010), a constant ratio of the adsorption-induced fracture strain increment to the sorption-induced coal bulk strain increment was introduced. By rearranging the Shi-Durucan model, they found that the ratio was significantly larger than (approximately 50 times) the sorption-induced coal bulk strain. Liu et al. (2010b) proposed the concept of elastic modulus reduction ratio to allocate matrix swelling strain to the fracture and the matrix. By assuming that only part of total swelling strain contributes to fracture aperture change and the remaining to coal bulk deformation, a permeability model under variable stress conditions was developed (Chen et al., 2012).

To explain the phenomenon of coal permeability switch from reduction to rebound under constant confining pressure condition, the concepts of critical pressure and critical time were introduced to define the switch from local swelling to macro-swelling due to gas diffusion from fractures to matrices (Liu et al., 2011b). Before the critical time, coal permeability was determined by the internal volumetric transformations (local swelling) between matrix swelling and fracture void compaction; after the critical time, coal permeability was determined by the external boundaries (macro-swelling). Similarly, the concept of critical swelling area was introduced to define the relation between swelling transition and coal permeability evolution under variable stress conditions (Qu et al., 2014). Subsequently, numerous coal permeability models were proposed (e.g. Guo et al., 2014; Wang et al., 2014; Peng et al., 2014b; Lu et al., 2016; Liu et al., 2017a). In these models, a constant strain splitting factor was used to define the ratio of the facture sorption strain to the matrix sorption strain. In a recent study (Peng et al., 2017a), the heterogeneous distribution of internal swelling was considered by extending the concept of strain splitting factor to strain splitting function. All strain splitting-based permeability models are summarized in Table 1. For sake of simplicity, only strain splitting-based parameters are presented in the table. More detailed information can be found in the original works.

As mentioned above, the impact of the differential strain between the fracture strain and the bulk strain is a challenging issue. To address this issue, a concept of differential swelling index (DSI) was introduced in this study to define the relation among sorption-induced deformations of the coal bulk, fracture, and coal matrix. Furthermore, a spectrum of DSI-based coal permeability models was developed to explicitly consider the effect of differential strains.

2. Concept of differential swelling index (DSI)

As shown in Introduction, coal permeability models can be classified into four categories. (1) The gas sorption-induced strain results in fracture strain only (Palmer and Mansoori, 1996; Shi and Durucan, 2003a); (2) The gas sorption-induced strain results in coal bulk strain only (Gray, 1987; Zhang et al., 2008); (3) The gas sorption-induced coal bulk strain equals the fracture strain (Zimmerman et al., 1986; Cui and Bustin, 2005); and (4) The ratio between two of the gas adsorption-induced three strain components (matrix strain, fracture strain and bulk strain) is a constant (Lu and Connell, 2010). The assumption that gas sorption-induced strain results in fracture strain only is not consistent with some experimental observations and significantly overestimates the effects of matrix swelling on permeability changes (Robertson, 2005). The assumption that adsorption only causes coal bulk strain, by contrast, would significantly underestimate the effect of adsorption. The third hypothesis that the adsorption-induced coal bulk strain is the same as the fracture strain may also underestimate the fracture strain (Connell et al., 2010b). The strain splitting approach (Zang et al., 2015; Peng et al., 2017a) is generally empirical. In following section, a theoretical approach is developed.

2.1. DSI model

Coal is a typical porous medium that consists of both matrices and fractures. In this study, the butt/face cleat system, fractures, bedding plies, and joints are all called the fracture system. Microscopic experimental techniques can be used to investigate sorption-induced strains in coal (Mao et al., 2015). It is found that with adsorption of gases, the matrix adsorption deformation makes

Table 1
Summary of strain splitting-based permeability models.

Expression	Parameter definition	Source
$\Delta\sigma = -\Delta P + \frac{E(f\Delta\varepsilon_s - \Delta\varepsilon_{fl})}{1-\nu}$	$f = \varepsilon_{SI}/\varepsilon_S$ is a constant between zero and one, and ε_{SI} is the internal swelling strain	Liu et al. (2010a)
$k = k_0 \exp[3(1-\gamma)\tilde{\varepsilon}_b^{(S)}]$	$\tilde{\varepsilon}_b^{(S)}$ is the coal bulk strain increment, and γ is the ratio between sorption-induced fracture strain and coal bulk strain.	Connell et al. (2010a)
$k/k_0 = \frac{k_{m0}}{k_{f0}+k_{m0}}\left(1+\frac{R_m}{\phi_{m0}}\frac{p_m}{K}\right)^3 + \frac{k_{f0}}{k_{f0}+k_{m0}}\left[1+\frac{1-R_m}{\phi_{m0}}(\Delta\varepsilon_V - \Delta\varepsilon_s)\right]^3$	R_m is the elastic modulus reduction ratio that represents the partition of the total strain	Liu et al. (2010b)
$k/k_0 = \begin{cases}\left[1+\frac{\alpha}{\phi_0}\left(-\Delta\varepsilon_s + \frac{p}{K_s}\right)\right]^3 & (p \le p_c)\\ \left[1+\frac{\alpha}{\phi_0}\left(-\frac{\varepsilon_L p_c}{p_c+P_L} + \frac{p_c}{K_s}\right)\right]^3\left[1+\frac{\alpha}{\phi_0}\left(\frac{p-p_c}{K}\right)\right]^3 & (p > p_c)\end{cases}$	p_c is the critical pressure	Liu et al. (2011)
$k/k_0 = \begin{cases}(1+\gamma\varepsilon_e)^3 & (k \le k_c)\\ (1+\beta\varepsilon_e)^3 & (k > k_c)\end{cases}$	k_c is the fracture permeability at the switching point	Qu et al. (2014)
$k/k_0 = e^{-3c_f\Delta(\bar{\sigma}-p)-3\beta\Delta\varepsilon_s}$	$\beta = 1 - A\frac{p-p_o}{P_c+p-p_0}$ is the strain splitting factor	Peng et al. (2017a)
$k/k_0 = [\exp(-C_f\Delta\sigma_e - S_f\Delta\varepsilon_s)]^3$	S_f is the ratio of fracture strain change to the incremental volumetric swelling strain	Chen et al. (2012)
$k/k_0 = \left\{1-\frac{\alpha}{\phi_0 K}[(\bar{\sigma}-\bar{\sigma}_0)-(P-P_0)] - \frac{f_m}{\phi_0}\left(\frac{\varepsilon_{max}P}{P+p_L} - \frac{\varepsilon_{max}P_0}{P_0+P_L}\right)\right\}^3$	$f_m = \frac{dV_{mf}}{dV_m}$ is the effective coal matrix deformation factor	Guo et al. (2014)
$k/k_0 = \exp\left\{-3c_f\left[(\bar{\sigma}-\bar{\sigma}_0)-(p-p_0)+f\frac{E}{3(1-2\nu)}\frac{\varepsilon^s_{max}p_\varepsilon(p-p_0)}{(p+p_\varepsilon)(p_0+p_\varepsilon)}\right]\right\}$	f defines the internal swelling partition	Lu et al. (2016)
$k/k_0 = \left[1-\frac{3f\varepsilon_L}{\phi_{f0}}\left(\frac{p_m}{p_L+p_m} - \frac{p}{p_L+p_{m0}}\right) - \frac{\sigma-\sigma_0-\alpha(p_f-p_{f0})-\beta(p_m-p_{m0})}{K_f}\right]^3$	f is the internal swelling coefficient	Liu et al. (2017b)
$k_z/k_{z0} = \left\{1+\frac{1}{\phi_0}\left[\frac{3(1-2\nu^b)(p-p_0)}{E^b} - \varepsilon_L\left(\frac{F_I p}{p_L+p} - \frac{F_{I0}p_0}{p_L+p_0}\right)\right]\right\}^3$	F_I is the internal swelling ratio	Wang et al. (2014)

the internal fracture compressed and the coal bulk swells (Karacan, 2003; Pone et al., 2009; Dawson et al., 2012). Three sorption-induced strains corresponding to three strain components were defined in this study: ε_b^s, ε_m^s, and ε_f^s, representing the sorption/desorption-induced coal bulk strain, matrix strain, and fracture strain, respectively. The adsorption-induced strain is the ratio of adsorption-caused volume fluctuations against original counterpart, which can be measured by a strain gage; the sorption-induced matrix strain, ε_m^s, can be measured for a small sample containing only coal matrix and no cleats; however, ε_f^s is more difficult to measure experimentally (Connell et al., 2010a). To study the microstructure of coal, micro-computed tomography (micro-CT) was applied (Ramandi et al., 2016), and it showed that coal is formed with a complex matrix-fracture system (Fig. 1a). A representative elementary volume (REV) of the coal structure is depicted in Fig. 1b, in which the value of initial coal bulk volume (V_{b0}) can be expressed by the sum of initial fracture volume (V_{f0}) and initial matrix volume (V_{m0}), i.e. $V_{b0}=V_{f0}+V_{m0}$. Coal adsorption characteristics can be generally measured under unconstrained conditions (Peng et al., 2017a). With gas adsorption, coal bulk swells and fracture is compressed. For the initial equilibrium stage as illustrated in Fig. 1c at the initial equilibrium pressure p_0, the volumes of coal bulk, matrix and fracture can be expressed as $V_{b0}(1+\varepsilon_b^s|_{p=p_0})$, $V_{m0}(1+\varepsilon_m^s|_{p=p_0})$, $V_{f0}(1+\varepsilon_f^s|_{p=p_0})$, respectively, where $\varepsilon_b^s|_{p=p_0}$, $\varepsilon_f^s|_{p=p_0}$, $\varepsilon_m^s|_{p=p_0}$ denote the adsorption-induced strains of coal bulk, coal fracture and coal matrix under pressure p_0, respectively. Similarly, as the pressure increases, the volume for the current equilibrium stage with equilibrium pressure p as shown in Fig. 1d can then be written as $V_{b0}(1+\varepsilon_b^s|_{p=p})$, $V_{m0}(1+\varepsilon_m^s|_{p=p})$, $V_{f0}(1+\varepsilon_f^s|_{p=p})$, respectively.

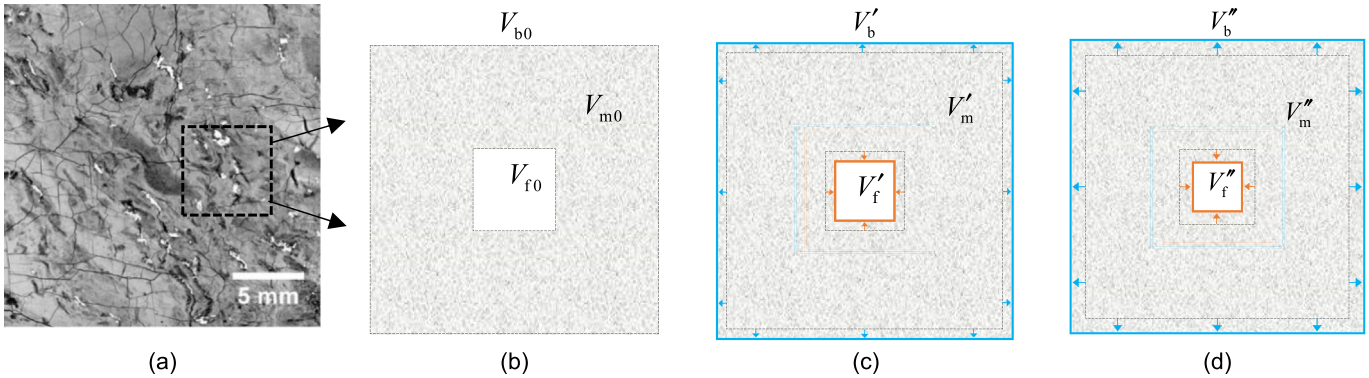

Fig. 1. Illustration of adsorption-induced differential swelling behavior: (a) Micro-CT image of coal structure (Ramandi et al., 2016); (b) representative elementary volume (REV); (c) Initial equilibrium stage (initial equilibrium pressure p_0); and (d) Current equilibrium stage (equilibrium pressure p).

By comparing the current stage and initial stage, we can obtain the volumetric balance between coal matrix, coal fracture and coal bulk:

$$V_{b0}\left(\varepsilon_b^s|_{p=p}-\varepsilon_b^s|_{p=p_0}\right)=V_{m0}\left(\varepsilon_m^s|_{p=p}-\varepsilon_m^s|_{p=p_0}\right)+V_{f0}\left(\varepsilon_f^s|_{p=p}-\varepsilon_f^s|_{p=p_0}\right) \quad (1)$$

Let $\Delta\varepsilon_b^s=\varepsilon_b^s|_{p=p}-\varepsilon_b^s|_{p=p_0}$ represent the increment of the coal bulk strain induced by adsorption, $\Delta\varepsilon_m^s=\varepsilon_m^s|_{p=p}-\varepsilon_m^s|_{p=p_0}$ represent the increment of the coal matrix strain, and $\Delta\varepsilon_f^s=\varepsilon_f^s|_{p=p}-\varepsilon_f^s|_{p=p_0}$ represent the increment of the coal fracture strain. Using the definition of porosity ($\phi=V_f/V_b$, where V_f is the fracture volume and V_b is the coal bulk volume), the relation between sorption-induced bulk strain increment, $\Delta\varepsilon_b^s$, matrix strain increment, $\Delta\varepsilon_m^s$, and fracture strain increment, $\Delta\varepsilon_f^s$, can be expressed as

$$\Delta\varepsilon_b^s=(1-\phi_0)\Delta\varepsilon_m^s+\phi_0\Delta\varepsilon_f^s \quad (2)$$

where ϕ_0 is the initial porosity.

Eq. (2) explicitly defines the relation among three strain components. Experimental data show that the measured matrix and coal bulk sorption strains can be fitted into Langmuir type curves (Harpalani and Schraufnagel, 1990b; Mitra et al., 2012; Wei et al., 2019b):

$$\varepsilon_s^i=\frac{\varepsilon_{Li}p}{p+P_{Li}} \quad (3)$$

where ε_s^i is the gas adsorption-induced strain; ε_L is the Langmuir strain constant that represents the maximum adsorption strain at infinite pressure; P_L is the Langmuir pressure constant at which the measured sorption strain is equal to $0.5\varepsilon_L$; and the subscript i = b and m denotes the bulk and matrix, respectively.

Although the fracture system controls the evolution of permeability, it is almost impossible to measure the adsorption strain of the fracture in experiment. The previous work on this issue has indicated that the value of pore strain was around 50 times the bulk strain for the coal under hydrostatic conditions (Connell et al., 2010b; Chen et al., 2012). As discussed above, the differential swelling/shrinking behavior defines the relation among the sorption-induced coal fracture, coal matrix and coal bulk strains. To further define the relation between $\Delta\varepsilon_b^s$ and ε_f^s, the differential swelling/shrinking index (DSI), f, was defined as $f=\Delta\varepsilon_f^s/\Delta\varepsilon_b^s$. Substituting the definition of coal swelling strain Eq. (3) into Eq. (2) gives

$$f=\frac{\Delta\varepsilon_f^s}{\Delta\varepsilon_b^s}=\frac{1}{\phi_0}\left[1-(1-\phi_0)\frac{\varepsilon_{Lm}P_{Lm}}{\varepsilon_{Lb}P_{Lb}}\frac{(p+P_{Lb})(p_0+P_{Lb})}{(p+P_{Lm})(p_0+P_{Lm})}\right] \quad (4)$$

In Eq. (4), DSI is a function of initial porosity, adsorption properties of coal matrix and coal bulk, and equilibrium pressure. All these parameters can be measured directly in laboratory. If the Langmuir pressure constants of coal bulk and coal matrix are assumed to be equal, i.e. $P_{Lb}=P_{Lm}$, the pressure-related terms on the right side of Eq. (4) disappear, then this index is degenerated into a constant ratio:

$$f^c=\frac{\Delta\varepsilon_f^s}{\Delta\varepsilon_b^s}=\frac{1}{\phi_0}\left[1-(1-\phi_0)\frac{\varepsilon_{Lm}}{\varepsilon_{Lb}}\right] \quad (5)$$

For this special case, the difference between Langmuir strain of coal matrix and coal bulk defines the differential swelling behavior. If the Langmuir strain constants are fixed, the ratios remain unchanged. This is consistent with the current assumptions (Lu and Connell, 2010; Chen et al., 2011). For the homogeneous case, all properties of the coal matrix and coal bulk are the same everywhere, i.e. $P_{Lm}=P_{Lb}$ and $\varepsilon_{Lm}=\varepsilon_{Lb}$. In this ideal case, DSI is equal to one, which is consistent with the theory of poroelasticity (Cui and Bustin, 2005; Zhang et al., 2008).

2.2. DSI-based permeability model

In this section, DSI was included in the coal permeability model. It is commonly assumed that the fracture system controls the gas flow in coal while the flow in the coal matrix can be neglected (Purl et al., 1991). Therefore, the evolution of permeability is mainly controlled by the behavior of fracture system (Sparks et al., 1995). Based on volumetric balance, the volumetric deformation of the coal bulk dV_b and the fracture dV_f consists of two parts (Gray, 1987; Connell et al., 2010a), i.e. one caused by effective stress dV_b^E and dV_f^E ($dV_b=dV_b^E+dV_b^S$), and the other by gas adsorption dV_b^S and dV_f^S ($dV_f=dV_f^E+dV_f^S$). Accordingly, for the strain increment, one can obtain that $d\varepsilon_b=d\varepsilon_b^E+d\varepsilon_b^S$ and $d\varepsilon_f=d\varepsilon_f^E+d\varepsilon_f^S$. Based on this, the volumetric strain of coal bulk (dV_b/V_b) and the volumetric strain of fractures (dV_f/V_f) can be expressed as follows (Detournay and Cheng, 1993; Zhang et al., 2008)

$$\frac{dV_b}{V_b}=-\frac{1}{K_b}(d\bar{\sigma}-\alpha dp)+d\varepsilon_b^s \quad (6)$$

$$\frac{dV_f}{V_f}=-\frac{1}{K_f}(d\bar{\sigma}-\beta dp)+d\varepsilon_f^s \quad (7)$$

where $\bar{\sigma}=-\sigma_{kk}/3$ is the mean compressive stress; K_b and K_f are the bulk moduli of coal bulk and coal fracture, respectively; and α and β are the Biot's coefficients. According to the definition of coal porosity, we deduce the following expression:

$$\frac{dV_b}{V_b}=\frac{dV_m}{V_m}+\frac{d\phi}{1-\phi} \quad (8)$$

$$\frac{dV_f}{V_f}=\frac{dV_m}{V_m}+\frac{d\phi}{(1-\phi)\phi} \quad (9)$$

Solving Eqs. (8) and (9), we obtain

$$\frac{d\phi}{\phi}=\frac{dV_f}{V_f}-\frac{dV_b}{V_b} \quad (10)$$

Substituting Eqs. (6) and (7) into Eq. (10) yields

$$\frac{d\phi}{\phi}=\left(\frac{1}{K_b}-\frac{1}{K_f}\right)d\bar{\sigma}+\left(\frac{1}{K_f}-\frac{1}{K_s}-\frac{\alpha}{K_b}\right)dp+d\varepsilon_f^s-d\varepsilon_b^s \quad (11)$$

As the bulk modulus K_b is commonly several orders of magnitude larger than the fracture volume modulus K_f (Peng et al., 2017a), by assuming that $1/K_b-1/K_f\approx-1/K_f$, the fracture compressibility can be defined as $c_f=1/K_f$ (Lu et al., 2016):

$$\frac{d\phi}{\phi}=-c_f d(\bar{\sigma}-p)+d\varepsilon_f^s-d\varepsilon_b^s \quad (12)$$

Integrating Eq. (12) with time gives

$$\frac{\phi}{\phi_0}=\exp\left\{-c_f[(\sigma_c-\sigma_{c0})-(p-p_0)]+\left(\Delta\varepsilon_f^s-\Delta\varepsilon_b^s\right)\right\} \quad (13)$$

By substituting the definition Eq. (4) of DSI into Eq. (13) yields

$$\frac{\phi}{\phi_0}=\exp\left\{-c_f[(\sigma_c-\sigma_{c0})-(p-p_0)]+(f-1)\Delta\varepsilon_b^s\right\} \tag{14}$$

The relationship between permeability and fracture porosity can be described by the cubic law (Chilingar, 1964; Chen et al., 2013; Cui et al., 2020) as

$$\frac{k}{k_0}=\left(\frac{\phi}{\phi_0}\right)^3 \tag{15}$$

where k is the permeability, and k_0 denotes the initial value of permeability.

Solving Eqs. (14) and (15), general form of the new permeability model can be expressed as

$$\frac{k}{k_0}=\exp\left\{-3c_f[(\sigma_c-\sigma_{c0})-(p-p_0)]+3(f-1)\cdot\left(\frac{\varepsilon_{Lb}p}{p+P_{Lb}}-\frac{\varepsilon_{Lb}p_0}{p_0+P_{Lb}}\right)\right\} \tag{16}$$

If equal adsorption-induced fracture and bulk strains are assumed (e.g. Cui and Bustin, 2005; Zhang et al., 2008), the adsorption-induced fracture and bulk strains cancel each other out. Assuming that the material is homogeneous, and the DSI is a constant ($f=1$), then the permeability model is degenerated as

$$\frac{k}{k_0}=\exp\left\{-3c_f[(\sigma_c-\sigma_{c0})-(p-p_0)]\right\} \tag{17}$$

Eq. (17) is the permeability model derived from the classical theory of poroelasticity.

2.3. Permeability models under different boundary conditions

The general permeability model defined by Eq. (16) can be applied to a range of boundary conditions from constant confining pressure to constant volume, as illustrated in Fig. 2.

2.3.1. Constant confining pressure condition

Under the constant confining pressure condition as shown in Fig. 2a, the change of the confining pressure ($\sigma_c-\sigma_{c0}$) is zero. In this circumstance, the permeability model can be expressed as

$$\frac{k}{k_0}=\exp\left[3c_f(p-p_0)+3(f-1)\left(\frac{\varepsilon_{Lb}p}{p+P_{Lb}}-\frac{\varepsilon_{Lb}p_0}{p_0+P_{Lb}}\right)\right] \tag{18}$$

By substituting DSI (Eq. (4)) into Eq. (18), the permeability model in the case of constant confining pressure in an expansion form is

$$\frac{k}{k_0}=\exp\left\{3c_f(p-p_0)+3\left\{\frac{1}{\phi_0}\left[1-(1-\phi_0)\frac{\varepsilon_{Lm}P_{Lm}}{\varepsilon_{Lb}P_{Lb}}\frac{(p+P_{Lb})(p_0+P_{Lb})}{(p+P_{Lm})(p_0+P_{Lm})}\right]-1\right\}\left(\frac{\varepsilon_{Lb}p}{p+P_{Lb}}-\frac{\varepsilon_{Lb}p_0}{p_0+P_{Lb}}\right)\right\} \tag{19}$$

2.3.2. Constant effective stress condition

For the case of constant effective stress condition as shown in Fig. 2b, the difference between confining stress and pore pressure remains constant and the increment of effective stress is equal to zero (Cui et al., 2018):

$$\Delta\sigma_e=(\sigma_c-\sigma_{c0})-(p-p_0) \tag{20}$$

Substituting Eq. (20) into Eq. (16), the permeability model for the case of constant effective stress becomes

$$\frac{k}{k_0}=\exp\left[3(f-1)\left(\frac{\varepsilon_{Lb}p}{p+P_{Lb}}-\frac{\varepsilon_{Lb}p_0}{p_0+P_{Lb}}\right)\right] \tag{21}$$

By substituting Eq. (4) into Eq. (21), the permeability model in an expansion form is

$$\frac{k}{k_0}=\exp\left\{3\left\{\frac{1}{\phi_0}\left[1-(1-\phi_0)\frac{\varepsilon_{Lm}P_{Lm}}{\varepsilon_{Lb}P_{Lb}}\frac{(p+P_{Lb})(p_0+P_{Lb})}{(p+P_{Lm})(p_0+P_{Lm})}\right]-1\right\}\cdot\left(\frac{\varepsilon_{Lb}p}{p+P_{Lb}}-\frac{\varepsilon_{Lb}p_0}{p_0+P_{Lb}}\right)\right\} \tag{22}$$

2.3.3. Uniaxial strain condition

For the case of uniaxial strain as shown in Fig. 2c, the vertical external stress remains constant ($\sigma_z-\sigma_{z0}=0$), the horizontal effective stress increments can be calculated by $\Delta\sigma_z^E=\sigma_z-\sigma_{z0}-(p-p_0)=-(p-p_0)$, and non-zero strain occurs in the vertical/axial direction and zero strain in the horizontal direction. The coal bulk volumetric strain increment can be represented as $\Delta\varepsilon_b=\Delta\varepsilon_{bx}+\Delta\varepsilon_{by}+\Delta\varepsilon_{bz}$. If the coal bulk strain induced by gas adsorption is isotropic ($\Delta\varepsilon_{bx}^s=\Delta\varepsilon_{by}^s=\Delta\varepsilon_{bz}^s=\Delta\varepsilon_b^s/3$), the coal bulk strain increment in three directions can be expressed as

$$\Delta\varepsilon_{bx}=\Delta\varepsilon_{bx}^E+\Delta\varepsilon_{bx}^S=-\frac{\Delta\sigma_x^E-\nu\Delta\sigma_y^E-\nu\Delta\sigma_z^E}{E}+\Delta\varepsilon_{bx}^s \tag{23a}$$

$$\Delta\varepsilon_{by}=\Delta\varepsilon_{by}^E+\Delta\varepsilon_{by}^S=-\frac{\Delta\sigma_y^E-\nu\Delta\sigma_x^E-\nu\Delta\sigma_z^E}{E}+\Delta\varepsilon_{by}^s \tag{23b}$$

$$\Delta\varepsilon_{bz}=\Delta\varepsilon_{bz}^E+\Delta\varepsilon_{bz}^S=-\frac{\Delta\sigma_z^E-\nu\Delta\sigma_x^E-\nu\Delta\sigma_y^E}{E}+\Delta\varepsilon_{bz}^s \tag{23c}$$

where ν is the Poisson's ratio, and E is the elastic modulus.

Substituting $\Delta\varepsilon_{bx}=\Delta\varepsilon_{by}=0$ and $\Delta\sigma_z^E=-\Delta p$ into Eq. (23a)-(23c), we can obtain the governing equation for the effective stress in horizontal direction:

$$\Delta\sigma_x^E=\Delta\sigma_y^E=\frac{E\Delta\varepsilon_b^s}{3(1-\nu)}-\frac{\nu}{1-\nu}(p-p_0) \tag{24}$$

Then the average effective stress imposed on the coal can be expressed as

$$\Delta\sigma_e=\frac{1}{3}\left(\Delta\sigma_x^E+\Delta\sigma_y^E+\Delta\sigma_z^E\right)=\frac{2E\Delta\varepsilon_b^s}{9(1-\nu)}-\frac{1+\nu}{3(1-\nu)}(p-p_0) \tag{25}$$

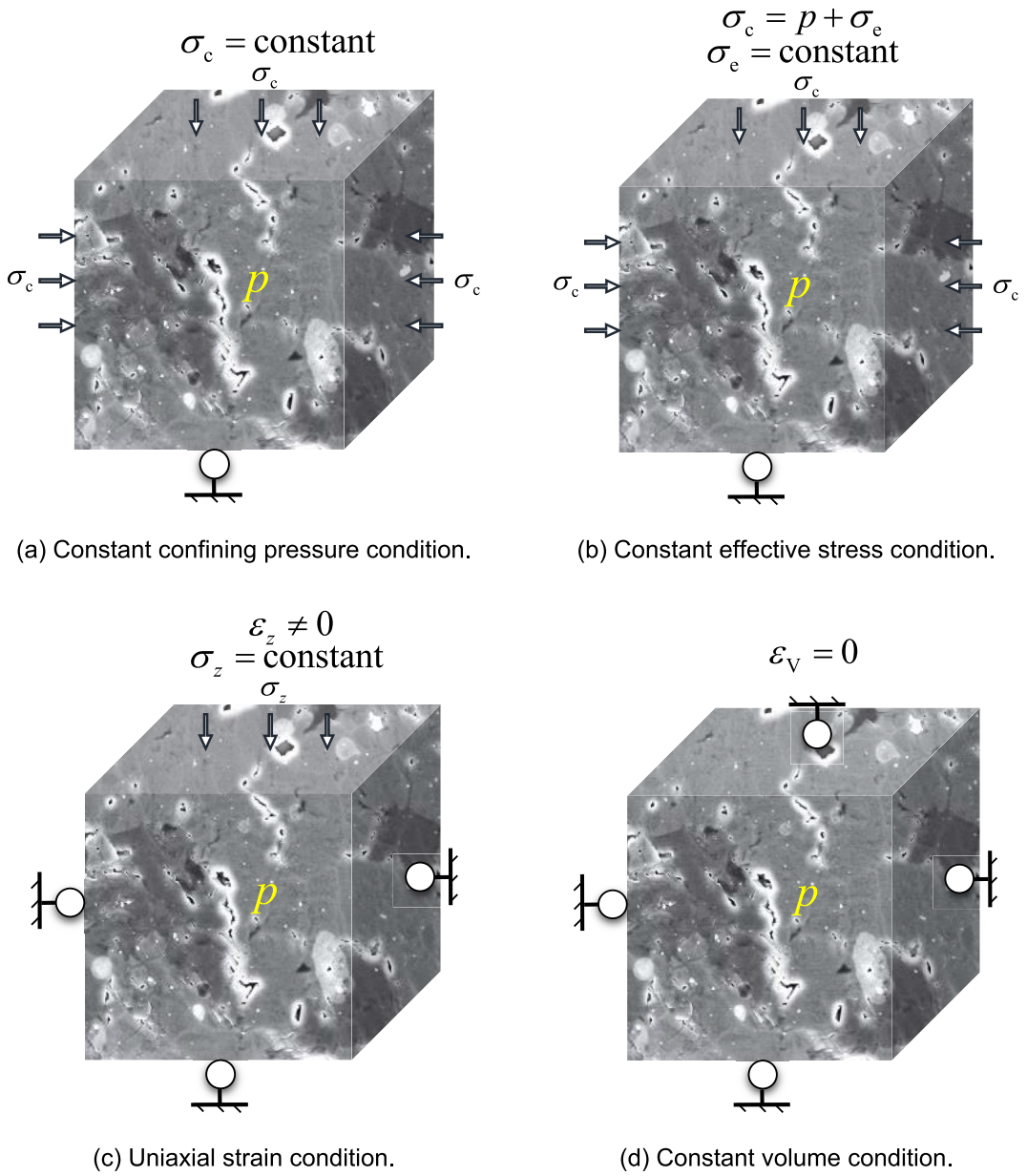

(a) Constant confining pressure condition.

(b) Constant effective stress condition.

(c) Uniaxial strain condition.

(d) Constant volume condition.

Fig. 2. Schematic diagrams of various boundary conditions.

Substituting Eq. (25) into Eq. (16), we can obtain the governing equation for the permeability change under the uniaxial strain condition:

$$\frac{k}{k_0} = \exp\left\{\frac{c_f(1+\nu)}{1-\nu}(p-p_0) + \left\{3\left\{\frac{1}{\phi_0}\left[1-(1-\phi_0)\frac{\varepsilon_{Lm}P_{Lm}}{\varepsilon_{Lb}P_{Lb}}\frac{(p+P_{Lb})(p_0+P_{Lb})}{(p+P_{Lm})(p_0+P_{Lm})}\right]-1\right\} - \frac{2c_fE}{3(1-\nu)}\right\}\left(\frac{\varepsilon_{Lb}p}{p+P_{Lb}} - \frac{\varepsilon_{Lb}p_0}{p_0+P_{Lb}}\right)\right\} \quad (27)$$

By substituting Eq. (4) into Eq. (26), the permeability model for the case of uniaxial strain in an expansion form is

$$\frac{k}{k_0} = \exp\left\{\frac{c_f(1+\nu)}{1-\nu}(p-p_0) + \left[3(f-1) - \frac{2c_fE}{3(1-\nu)}\right] \cdot \left(\frac{\varepsilon_{Lb}p}{p+P_{Lb}} - \frac{\varepsilon_{Lb}p_0}{p_0+P_{Lb}}\right)\right\} \quad (26)$$

2.3.4. Constant volume condition

For the case constant volume condition as shown in Fig. 2d, the displacement of coal sample in each direction is zero, i.e. the total volume of coal remains unchanged. Then, the coal bulk

strain increment is zero ($d\varepsilon_b = dV_b/V_{b0} = 0$), and sorption-induced matrix strain contributes to fracture deformation only. Ma et al. (2011) developed a permeability model under the constant volume boundary condition by making a distinction between mechanical compression-induced strain and matrix shrinking strain. In the experiment, the expansion of coal is controlled by adjusting confining pressure to achieve the goal of constant volume boundary condition (Espinoza et al., 2014). Based on above understanding, substituting $d\varepsilon_b = 0$ into Eq. (6) yields

$$d\varepsilon_b^s = \frac{1}{K_b}(d\bar{\sigma} - \alpha dp) \tag{28}$$

Assuming Biot's coefficient $\alpha = 1$, we can obtain $K_b d\varepsilon_b^s = d\bar{\sigma} - dp$. Substituting this relation and $d\varepsilon_b = 0$ into Eq. (11) yields

$$\frac{d\phi}{\phi} = \frac{dV_f}{V_f} = -c_f K_b d\varepsilon_b^s + d\varepsilon_f^s \tag{29}$$

Integrating Eq. (29) gives porosity model for the case of constant volume:

$$\frac{\phi}{\phi_0} = \exp\left(-c_f K_b \Delta\varepsilon_b^s + \Delta\varepsilon_f^s\right) \tag{30}$$

Based on the cubic law and by substituting the DSI into the porosity model, we can obtain the governing equation for the permeability change under the constant volume condition:

$$\frac{k}{k_0} = \exp\left[\left(-c_f\frac{E}{1-2\nu} + 3f\right)\left(\frac{\varepsilon_{Lb}p}{p+P_{Lb}} - \frac{\varepsilon_{Lb}p_0}{p_0+P_{Lb}}\right)\right] \tag{31}$$

By substituting Eq. (4) into Eq. (31), the permeability model for the case of constant volume can be defined in an expansion form as

$$\frac{k}{k_0} = \exp\left\{\left\{-c_f\frac{E}{1-2\nu} + 3\frac{1}{\phi_0}\left[1-(1-\phi_0)\frac{\varepsilon_{Lm}P_{Lm}}{\varepsilon_{Lb}P_{Lb}}\frac{(p+P_{Lb})(p_0+P_{Lb})}{(p+P_{Lm})(p_0+P_{Lm})}\right]\right\}\left(\frac{\varepsilon_{Lb}p}{p+P_{Lb}} - \frac{\varepsilon_{Lb}p_0}{p_0+P_{Lb}}\right)\right\} \tag{32}$$

3. Model verifications

In this section, our models are compared with experimental observations under a spectrum of boundary conditions from constant confining pressure to uniaxial strain. Four sets of experimental data under these boundary conditions (Robertson and Christiansen, 2005; Pini et al., 2009; Connell et al., 2010a; Mitra et al., 2012) were used. In addition, we also compared with the performances of other models for the same data sets (Connell et al., 2010a; Guo et al., 2014).

Table 2
Properties of coal and fluid for the experiment conducted by Pini et al. (2009).

Symbol	Description	Value	Unit
ϕ_0	Initial porosity	0.42	%
ε_L^b	Langmuir strain constant of coal bulk	0.049	
P_L^b	Langmuir pressure constant of coal bulk	2.631	MPa
c_f	Fracture compressibility	0.1896	MPa^{-1}
ε_L^m	Langmuir strain constant of coal matrix	0.0556	
P_L^m	Langmuir pressure constant of coal matrix	2.631	MPa

Table 3
Properties of Anderson coal for the experiment conducted by Robertson and Christiansen (2005).

Symbol	Description	Value	Unit
ϕ_0	Initial porosity	1.31	%
ε_L^b	Langmuir strain constant of coal bulk	0.00931	
P_L^b	Langmuir pressure constant of coal bulk	6.11	MPa
c_f	Fracture compressibility	0.058	MPa^{-1}
ε_L^m	Langmuir strain constant of coal matrix	0.0139	
P_L^m	Langmuir pressure constant of coal matrix	2.487	MPa

3.1. Constant confining pressure condition

We compared the model results of Eq. (19) with experimental data under constant confining pressure condition (Robertson and Christiansen, 2005; Pini et al., 2009). Basic parameters for the experiments are listed in Tables 2 and 3. The matrix Langmuir adsorption constants of ε_{Lm} and P_{Lm} were obtained by matching the experimental data. The comparisons of our model against experimental data are illustrated in Figs. 3 and 4.

As shown in Fig. 3, our model results matched the permeability data well for the Sulcis coal. In this case, $P_{Lm} = 2.631$ MPa, $\varepsilon_{Lm} = 0.0556$, and the Langmuir pressure constant for the matrix and coal bulk were equal ($P_{Lm} = P_{Lb}$). Under these conditions, the DSI was a constant ($f = -26.93$). This indicates that the ratio of the adsorption-induced fracture strain increment to the bulk strain increment remains unchanged as the gas pressure increases. We also compared our model results with the results of the model proposed by Connell et al. (2010a). In this particular case, two lines were overlapped because of the same DSI value ($f = \gamma = -26.93$). As shown in Fig. 4, our new model results also match the permeability data for the Anderson coal. In this case ($P_{Lm} = 2.3$ MPa, $\varepsilon_{Lm} = 0.041$), the DSI value decreases as the gas pressure increases.

3.2. Constant effective stress condition

We compared our model performance of Eq. (22) with the experimental data (Connell et al., 2010a) for the case of constant effective stress, as shown in Fig. 5. The mechanical parameters and the adsorption constants, as listed in Table 4, were taken directly from this study (Connell et al., 2010a). The permeability data were extracted from the original figures using a data extractor. Compared with the original data, there might be some imperceptible errors, but it will not affect the overall trend and the verification process. In this case ($P_{Lm} = 15.9$ MPa and $\varepsilon_{Lm} = 0.022$), our new model results matched experimental data very well for the coal sample from Southern Sydney basin. The value of the DSI increases as the gas pressure increases. If a constant DSI value is used, with $\gamma = -18.7$ and $\gamma = -26.2$, the matches are less satisfactory.

3.3. Uniaxial strain condition

We compared our model performance of Eq. (27) with the experimental data (Mitra et al., 2012) for the case of uniaxial strain, as shown in Fig. 6. The parameters are listed in Table 5. It should be noted that the initial porosity, elastic modulus and Poisson's

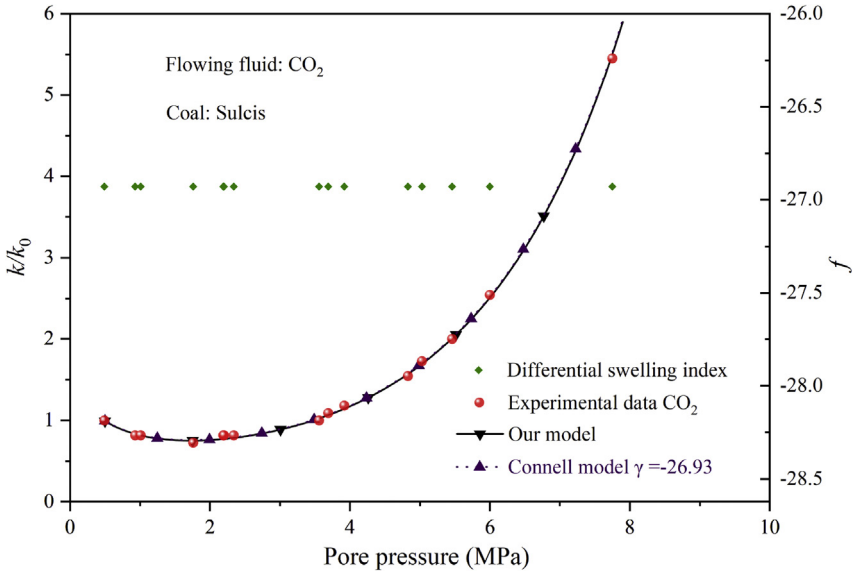

Fig. 3. Comparisons of our model results with experimental data for the Sulcis coal sample (Pini et al., 2009).

ratio were not provided in their study, thus we used the initial porosity from Young et al. (1991), elastic modulus and Poisson's ratio from Shi et al. (2005). As shown in Fig. 6, our model results matched well with the experimental data. In this case (P_{Lm} = 2.795 MPa and ε_{Lm} = 0.0195), the DSI value f decreased with the pressure. As shown in Fig. 6, we also compared the performance of our model with others including SD model, modified SD model (Liu et al., 2012), and our constant DSI model.

4. Discussion

As shown in Section 3, the DSI plays a key role in comparison of our model results with experimental data. Unlike previous studies, f is a function of gas pressure and regulated by Langmuir constants (P_{Lm} and P_{Lb}; ε_{Lm} and ε_{Lb}) for both matrices and coal bulk, respectively.

In the following, all of the input parameters are taken from Mitra et al. (2012) and are listed in Table 3, and an initial gas pressure (p_0 = 0.5 MPa) is assumed. The DSI was calculated by use of Eq. (4). Note that the Langmuir pressure constant is P_{Lb} = 4.16 MPa for the experiment data. By changing the matrix Langmuir pressure constant P_{Lm}, we can obtain the evolution trends of f, as shown in Fig. 7a. The corresponding evolutions of permeability under constant confining pressure, constant effective stress and uniaxial strain conditions are shown in Fig. 7b–d, respectively.

As shown in Fig. 7a, f decreases as pressure increases when $P_{Lm} < P_{Lb}$, f increases as pressure increases when $P_{Lm} > P_{Lb}$, and f remains as a constant when $P_{Lm} = P_{Lb}$. As shown in Fig. 7b–d,

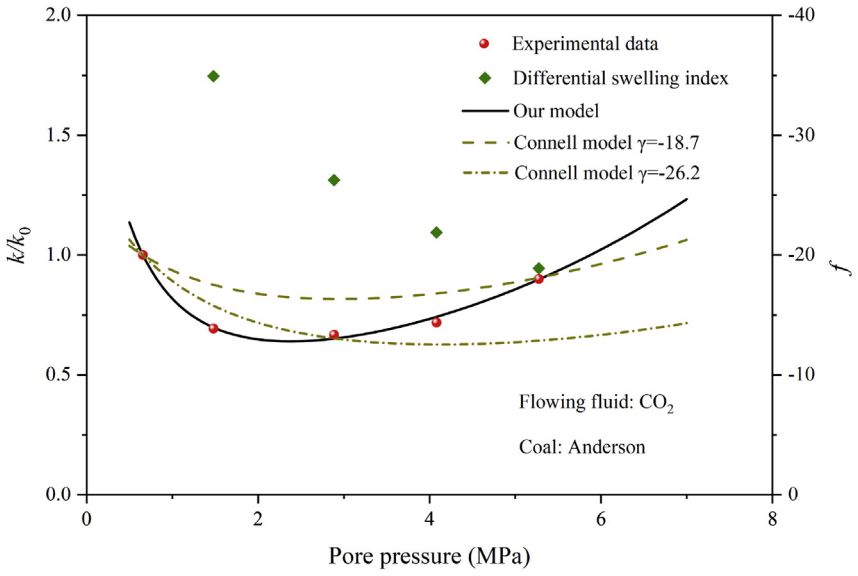

Fig. 4. Comparisons of our model results with the experimental data for the Anderson coal sample (Robertson and Christiansen, 2005).

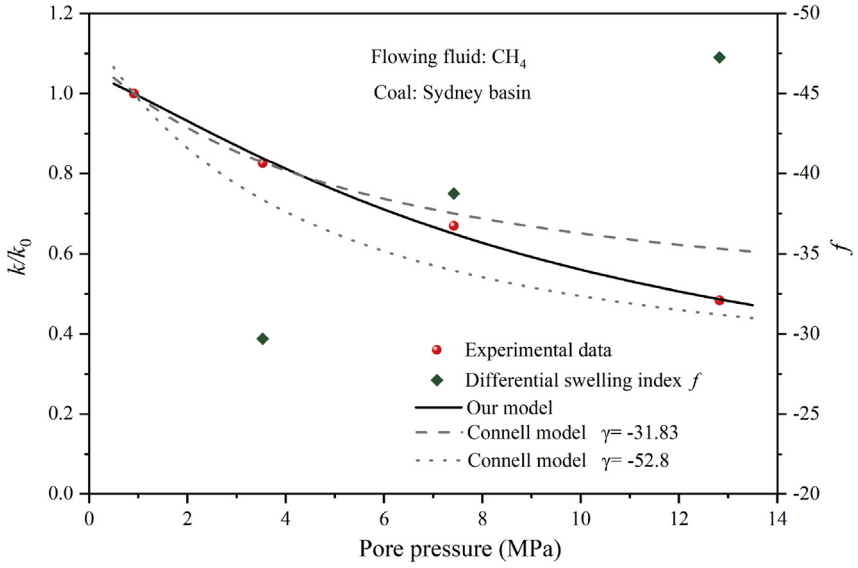

Fig. 5. Comparisons between different model results and the experimental data under constant effective stress condition for Southern Sydney basin coal sample (Connell et al., 2010a).

Table 4
Parameters used in matching the permeability for coal core sample from the Southern Sydney basin of Australia.

Symbol	Description	Value	Unit
ϕ_0	Initial porosity	1.5	%
ε_L^b	Langmuir strain constant of coal bulk	0.01	
P_L^b	Langmuir pressure constant of coal bulk	8.9	MPa
c_f	Fracture compressibility	0.058	MPa^{-1}
ε_L^m	Langmuir strain constant of coal matrix	0.022	
P_L^m	Langmuir pressure constant of coal matrix	15.9	MPa

the magnitudes of f have a significant impact on the evolutions of coal permeability under different boundary conditions. For example, coal permeability decreases initially and then recovers as pressure increases when $P_{Lm} < P_{Lb}$, and coal permeability increases continuously as pressure increases when $P_{Lm} > P_{Lb}$. These model results illustrate that matrix Langmuir constants control the evolution of coal permeability.

Table 5
Parameters for data matching under uniaxial strain condition (Mitra et al., 2012).

Symbol	Description	Value	Unit
ϕ_0	Initial porosity	0.75	%
ε_L^b	Langmuir strain constant of coal bulk	0.01075	
P_L^b	Langmuir pressure constant of coal bulk	4.16	MPa
c_f	Fracture compressibility	0.092	MPa^{-1}
E	Elastic modulus	2902	MPa
ν	Poisson's ratio	0.35	
ε_L^m	Langmuir strain constant of coal matrix	0.0195	
P_L^m	Langmuir pressure constant of coal matrix	2.795	MPa
p_0	Initial equilibrium pressure	6.25	MPa

As shown in Eq. (4), f is a function of pressure only and independent of boundary conditions. Under the same pressures, we calculated all permeability evolutions for a range of boundary conditions from constant confining stress to constant volume conditions, as shown in Fig. 8. The upper envelope is the

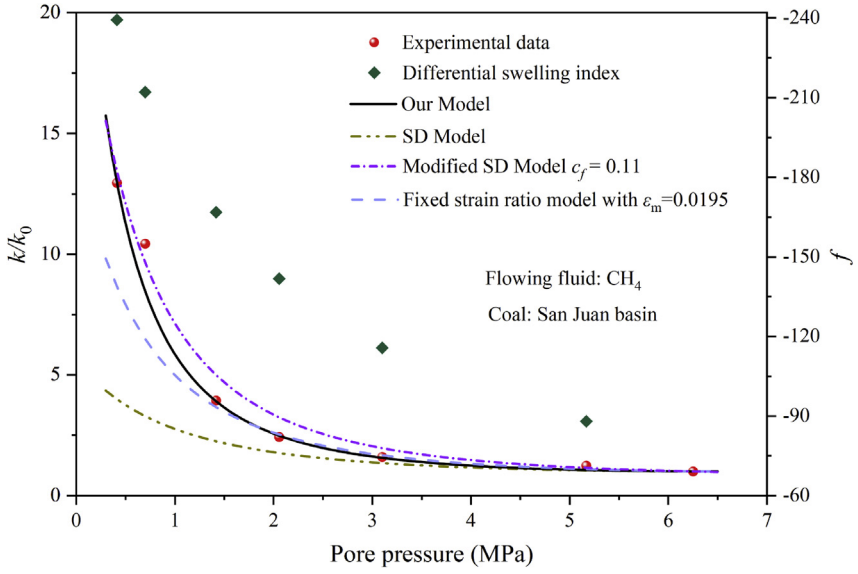

Fig. 6. Comparisons between different model results and the experimental data under uniaxial strain condition for San Juan basin coal sample (Mitra et al., 2012).

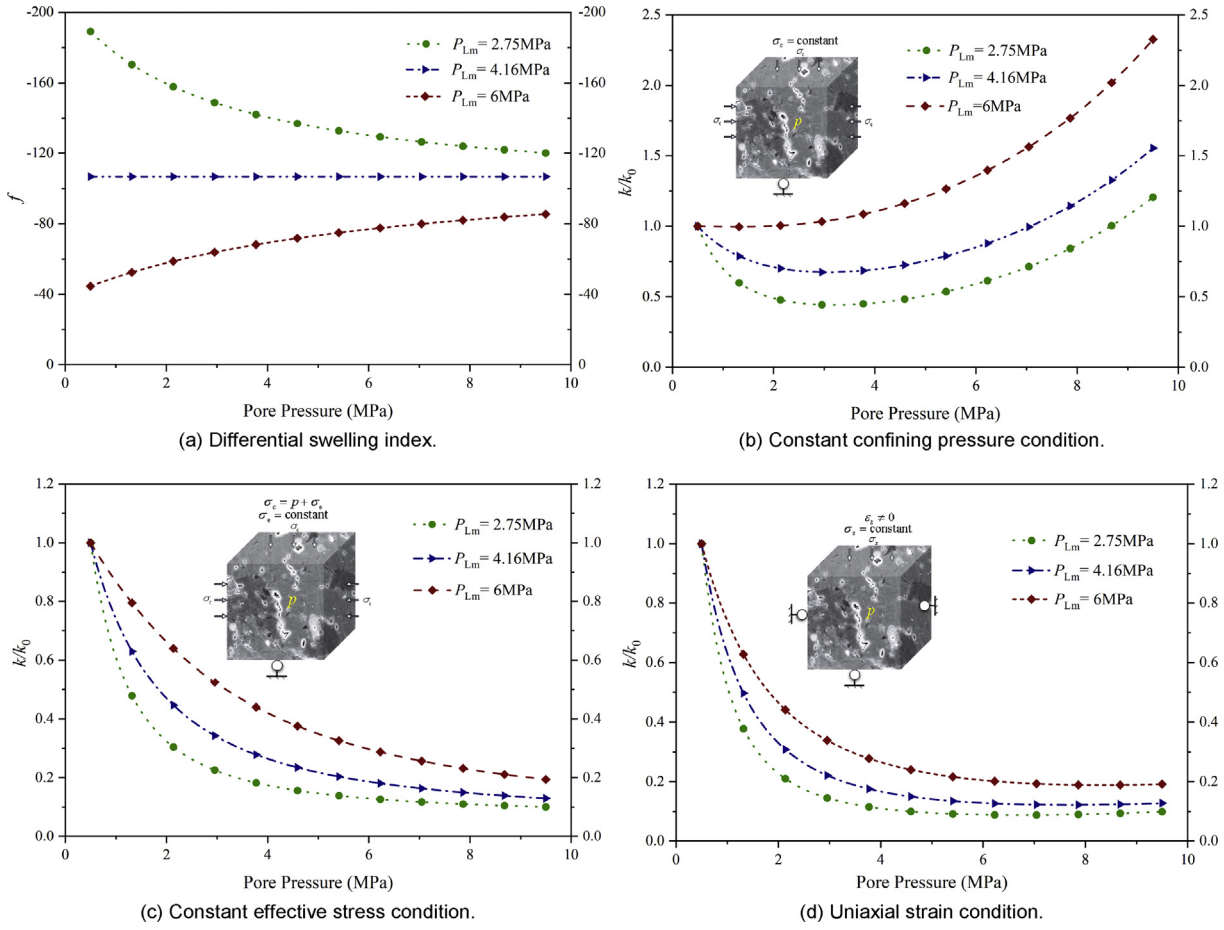

Fig. 7. Permeability evolution with different differential swelling index.

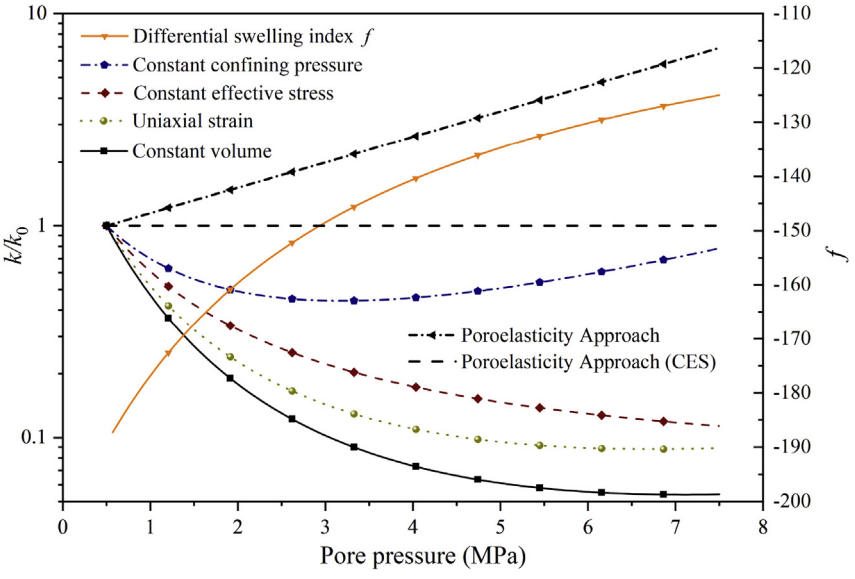

Fig. 8. Permeability model evolution under different boundary conditions.

conventional poroelasticity solution for the case of constant confining stress, while the lower envelope is the conventional poroelasticity solution for the case of constant volume condition. Solutions of all other cases are within these envelopes.

5. Conclusions

In this study, a concept of DSI is proposed to theoretically define the relation among sorption-induced strains of the coal bulk,

fracture and matrix at the equilibrium state. DSI is a function of the equilibrium pressure and its magnitudes are regulated by the Langmuir constants of both the coal matrix and the coal bulk. Furthermore, a spectrum of DSI-based coal permeability models is developed to explicitly consider the effect of differential strains. These models are verified with the experimental data under the conditions of uniaxial strain, constant confining pressure and constant effective stress. Based on the model results and verifications, the following conclusions can be drawn:

(1) When the gas sorption-induced fracture strain is assumed the same as the bulk strain, DSI is equal to unity; when the Langmuir constants for matrix are the same as the ones for coal bulk, DSI is a constant. However, DSI is a function of the equilibrium pressure when the Langmuir constants for matrix are different from the ones for coal bulk. The theoretical development of DSI concept essentially removes the basic assumptions in previous studies.
(2) An equilibrium state is typically assumed when interpreting permeability measurements – representing the assumption that equilibration has been reached and that both sorption-induced changes in deformation and their impacts on the evolution of permeability have ceased. At the equilibrium state, coal permeability is a function of equilibrium pressure and its magnitudes are regulated by the magnitudes of DSI.

Declaration of Competing Interest

The authors wish to confirm that there are no known conflicts of interest associated with this publication and there has been no significant financial support for this work that could have influenced its outcome.

Acknowledgments

This work was supported by National Key R&D Program of China (Grant No. 2018YFC0407006), the 111 Project (Grant No. B17009), and the Australian Research Council (Grant No. DP200101293). These supports are gratefully acknowledged.

References

Chen D, Pan Z, Liu J, Connell LD. An improved relative permeability model for coal reservoirs. International Journal of Coal Geology 2013;109:45–57.
Chen T, Feng X, Cui G, Tan Y, Pan Z. Experimental study of permeability change of organic-rich gas shales under high effective stress. Journal of Natural Gas Science and Engineering 2019;64:1–14.
Chen Z, Liu J, Pan Z, Connell LD, Elsworth D. Influence of the effective stress coefficient and sorption-induced strain on the evolution of coal permeability: model development and analysis. International Journal of Greenhouse Gas Control 2012;8(5):101–10.
Chen Z, Pan Z, Liu J, Connell LD, Elsworth D. Effect of the effective stress coefficient and sorption-induced strain on the evolution of coal permeability: experimental observations. International Journal of Greenhouse Gas Control 2011;5(5):1284–93.
Chilingar GV. Relationship between porosity, permeability, and grain-size distribution of sands and sandstones. In: Developments in sedimentology. Elsevier; 1964.
Connell LD, Lu M, Pan Z. An analytical coal permeability model for tri-axial strain and stress conditions. International Journal of Coal Geology 2010a;84(2):103–14.
Connell LD, Pan Z, Lu M, Heryanto DD, Camilleri M. Coal permeability and its behaviour with gas desorption, pressure and stress. In: SPE asia pacific oil and gas conference and exhibition. Society of Petroleum Engineers (SPE); 2010b.
Cui G, Liu J, Wei M, Shi R, Elsworth D. Why shale permeability changes under variable effective stresses: new insights. Fuel 2018;213:55–71.
Cui G, Feng X, Pan Z, Chen T, Liu J, Elsworth D, Tan Y, Wang C. Engineering. Impact of shale matrix mechanical interactions on gas transport during production. Journal of Natural Gas Science and Engineering 2020;184:106524. https://doi.org/10.1029/2004JB003482.
Cui X, Bustin RM. Volumetric strain associated with methane desorption and its impact on coalbed gas production from deep coal seams. AAPG Bulletin 2005;89(9):1181–202.
Cui X, Bustin RM, Chikatamarla L. Adsorption-induced coal swelling and stress: implications for methane production and acid gas sequestration into coal seams. Journal of Geophysical Research 2007;112(B10).
Dawson G, Golding S, Esterle J, Massarotto P. Occurrence of minerals within fractures and matrix of selected Bowen and Ruhr Basin coals. International Journal of Coal Geology 2012;94:150–66.
Detournay E, Cheng AHD. Fundamentals of poroelasticity. In: Analysis and design methods. Elsevier; 1993.
Espinoza DN, Vandamme M, Pereira JM, Dangla P, Vidal-Gilbert S. Measurement and modeling of adsorptive–poromechanical properties of bituminous coal cores exposed to CO_2: adsorption, swelling strains, swelling stresses and impact on fracture permeability. International Journal of Coal Geology 2014;134–135:80–95.
Flores RM. Coalbed methane: from hazard to resource. International Journal of Coal Geology 1998;35(1–4):3–26.
Gierhart RR, Clarkson CR, Seidle JP. Spatial variation of San Juan Basin Fruitland coalbed methane pressure dependent permeability: magnitude and functional form. In: International petroleum technology conference; 2007.
Gray I. Reservoir engineering in coal seams: Part 1-The physical process of gas storage and movement in coal seams. SPE Reservoir Engineering 1987;2(1):28–34.
Gunter W, Gentzis T, Rottenfusser B, Richardson R. Deep coalbed methane in Alberta, Canada: a fuel resource with the potential of zero greenhouse gas emissions. Energy Conversion and Management 1997;38:S217–22.
Guo P, Cheng Y, Jin K, Li W, Tu Q, Liu H. Impact of effective stress and matrix deformation on the coal fracture permeability. Transport in Porous Media 2014;103(1):99–115.
Harpalani S, Schraufnagel RA. Shrinkage of coal matrix with release of gas and its impact on permeability of coal. Fuel 1990a;69(5):551–6.
Harpalani S, Schraufnagel A. Measurement of parameters impacting methane recovery from coal seams. International Journal of Mining and Geological Engineering 1990b;8(4):369–84.
Karacan CÖ. Heterogeneous sorption and swelling in a confined and stressed coal during CO_2 injection. Energy & Fuels 2003;17(6):1595–608.
Lin W, Kovscek AR. Gas sorption and the consequent volumetric and permeability change of coal. I: Experimental. Transport in Porous Media 2014;105(2):371–89.
Liu HH, Rutqvist J, Oldenburg CM. A new coal-permeability model: internal swelling stress and fracture-matrix interaction. Transport in Porous Media 2010a;82(1):157–71.
Liu J, Chen Z, Elsworth D, Miao X, Mao X. Linking gas-sorption induced changes in coal permeability to directional strains through a modulus reduction ratio. International Journal of Coal Geology 2010b;83(1):21–30.
Liu J, Wang J, Chen Z, Wang S, Elsworth D, Jiang Y. Impact of transition from local swelling to macro swelling on the evolution of coal permeability. International Journal of Coal Geology 2011;88(1):31–40.
Liu S, Harpalani S, Pillalamarry M. Laboratory measurement and modeling of coal permeability with continued methane production: Part 2 – modeling results. Fuel 2012;94:117–24.
Liu T, Lin B, Yang W, Zhai C, Liu T. Coal Permeability evolution and gas migration under non-equilibrium state. Transport in Porous Media 2017a;118(3):393–416.
Liu T, Lin B, Yang W. Impact of matrix–fracture interactions on coal permeability: model development and analysis. Fuel 2017b;207:522–32.
Lu M, Connell LD. Swell of coal matrix induced by gas sorption and its partition to pore volume and bulk strains - a critical parameter for coal permeability. In: Proceedings of the 44th US rock mechanics symposium and 5th US-Canada rock mechanics symposium. American Rock Mechanics Association (ARMA); 2010.
Lu S, Cheng Y, Li W. Model development and analysis of the evolution of coal permeability under different boundary conditions. Journal of Natural Gas Science and Engineering 2016;31:129–38.
Ma Q, Harpalani S, Liu S. A simplified permeability model for coalbed methane reservoirs based on matchstick strain and constant volume theory. International Journal of Coal Geology 2011;85(1):43–8.
Mao L, Hao N, An L, Chiang F-P, Liu H. 3D mapping of carbon dioxide-induced strain in coal using digital volumetric speckle photography technique and X-ray computer tomography. International Journal of Coal Geology 2015;147–148:115–25.
Meng Y, Li Z, Lai F. Experimental study on porosity and permeability of anthracite coal under different stresses. Journal of Petroleum Science & Engineering 2015;133:810–7.
Mitra A, Harpalani S, Liu S. Laboratory measurement and modeling of coal permeability with continued methane production: Part 1 – laboratory results. Fuel 2012;94:110–6.
Moore TA. Coalbed methane: a review. International Journal of Coal Geology 2012;101:36–81.
Palmer I, Mansoori J. How permeability depends on stress and pore pressure in coalbeds: a new model. In: SPE annual technical conference and exhibition. Society of Petroleum Engineers (SPE); 1996.
Peng Y, Liu J, Pan Z, Connell LD, Chen Z, Qu H. Impact of coal matrix strains on the evolution of permeability. Fuel 2017a;189:270–83.
Peng Y, Liu J, Wei M, Pan Z, Connell LD. Why coal permeability changes under free swellings: new insights. International Journal of Coal Geology 2014b;133:35–46.

Perera MSA, Ranjith P, Choi S. Coal cleat permeability for gas movement under triaxial, non-zero lateral strain condition: a theoretical and experimental study. Fuel 2013;109:389–99.
Pini R, Ottiger S, Burlini L, Storti G, Mazzotti M. Role of adsorption and swelling on the dynamics of gas injection in coal. Journal of Geophysical Research: Solid Earth 2009;114(B4). https://doi.org/10.1029/2008JB005961.
Pone JDN, Hile M, Halleck PM, Mathews JP. Three-dimensional carbon dioxide-induced strain distribution within a confined bituminous coal. International Journal of Coal Geology 2009;77(1–2):103–8.
Puri R, Yee D. Enhanced coalbed methane recovery. In: SPE annual technical conference and exhibition. Society of Petroleum Engineers (SPE); 1990.
Purl R, Evanoff J, Brugler M. Measurement of coal cleat porosity and relative permeability characteristics. In: SPE gas technology symposium. Society of Petroleum Engineers (SPE); 1991.
Qu H, Liu J, Pan Z, Connell L. Impact of matrix swelling area propagation on the evolution of coal permeability under coupled multiple processes. Journal of Natural Gas Science & Engineering 2014;18:451–66.
Ramandi HL, Mostaghimi P, Armstrong RT, Saadatfar M, Pinczewski WV. Porosity and permeability characterization of coal: a micro-computed tomography study. International Journal of Coal Geology 2016;154–155:57–68.
Robertson EP. Measurement and modeling of sorption-induced strain and permeability changes in coal. PhD Thesis. Colorado School of Mines; 2005.
Robertson EP, Christiansen RL. Modeling permeability in coal using sorption-induced strain data. In: SPE annual technical conference and exhibition. Society of Petroleum Engineers (SPE); 2005.
Shi JQ, Durucan S. A model for changes in coalbed permeability during primary and enhanced methane recovery. SPE Reservoir Evaluation & Engineering 2005;8(4):291–9.
Shi J, Durucan S. Changes in permeability of coalbeds during primary recovery–part 1: model formulation and analysis. In: Proceedings of the 2003 international coalbed methane symposium. University of Alabama; 2003a.
Shi JQ, Durucan S. A bidisperse pore diffusion model for methane displacement desorption in coal by CO_2 injection. Fuel 2003b;82(10):1219–29.
Shi R, Liu J, Wei M, Elsworth D, Wang X. Mechanistic analysis of coal permeability evolution data under stress-controlled conditions. International Journal of Rock Mechanics and Mining Sciences 2018;110:36–47.
Siriwardane H, Haljasmaa I, McLendon R, Irdi G, Soong Y, Bromhal G. Influence of carbon dioxide on coal permeability determined by pressure transient methods. International Journal of Coal Geology 2009;77(1):109–18.
Sparks D, McLendon T, Saulsberry J, Lambert S. The effects of stress on coalbed reservoir performance, Black Warrior Basin, USA. In: SPE annual technical conference and exhibition. Society of Petroleum Engineers (SPE); 1995.
Vishal V, Ranjith PG, Pradhan SP, Singh TN. Permeability of sub-critical carbon dioxide in naturally fractured Indian bituminous coal at a range of down-hole stress conditions. Engineering Geology 2013;167:148–56.
Wang C, Zhai P, Chen Z, Liu J, Wang L, Xie J. Experimental study of coal matrix-cleat interaction under constant volume boundary condition. International Journal of Coal Geology 2017;181:124–32.
Wang K, Zang J, Wang G, Zhou A. Anisotropic permeability evolution of coal with effective stress variation and gas sorption: model development and analysis. International Journal of Coal Geology 2014;130:53–65.
Wang L, Chen Z, Wang C, Elsworth D, Liu W. Reassessment of coal permeability evolution using steady-state flow methods: the role of flow regime transition. International Journal of Coal Geology 2019;211:103210. https://doi.org/10.1016/j.coal.2019.103210.
Wang S, Elsworth D, Liu J. Permeability evolution in fractured coal: the roles of fracture geometry and water-content. International Journal of Coal Geology 2011;87(1):13–25.
Wei M, Liu J, Shi R, Elsworth D, Liu Z. Long-term evolution of coal permeability under effective stresses gap between matrix and fracture during CO_2 injection. Transport in Porous Media 2019a;130(3):1–15.
Wei M, Liu Y, Liu J, Elsworth D, Zhou F. Micro-scale investigation on coupling of gas diffusion and mechanical deformation of shale. Journal of Petroleum Science Engineering 2019b;175:961–70.
Young G, McElhiney J, Paul G, McBane R. An analysis of Fruitland coalbed methane production, Cedar Hill field, northern San Juan Basin. In: SPE annual technical conference and exhibition. Society of Petroleum Engineers (SPE); 1991.
Zang J, Wang K, Zhao Y. Evaluation of gas sorption-induced internal swelling in coal. Fuel 2015;143:165–72.
Zhang H, Liu J, Elsworth D. How sorption-induced matrix deformation affects gas flow in coal seams: a new FE model. International Journal of Rock Mechanics and Mining Sciences 2008;45(8):1226–36.
Zimmerman RW, Somerton WH, King MS. Compressibility of porous rocks. Journal of Geophysical Research: Solid Earth 1986;91(B12):12765–77.

Jishan Liu is professor of the Department of Chemical Engineering, School of Engineering, The University of Western Australia. Liu received his PhD in Mining Engineering from Penn State University, USA, in 1996. After that, he has been working primarily at the University of Western Australia. His research interests cover Unconventional Reservoir Multiphysics (URM) with an application to coal seam gas extraction, shale gas extraction, stacked deposits extraction, CO_2 sequestration in coal, coal mine safety, and caprock sealing safety.